Double Layers and Ion Phase-Space Holes in the Auroral Upward-Current Region

D. S. Main,[1,*] D. L. Newman,[2] and R. E. Ergun[1]

[1]*Laboratory for Atmospheric and Space Physics, University of Colorado at Boulder, Boulder, Colorado 80309, USA*
[2]*Center for Integrated Plasma Studies, University of Colorado at Boulder, Boulder, Colorado 80309, USA*

The dynamic evolution of the boundary between the ionosphere and auroral cavity is studied using 1D and 2D kinetic Vlasov simulations. The initial distributions of three singly ionized species (H^+, O^+, e^-) are determined from space-based observations on both sides of an inferred strong double layer. The kinetic simulations reproduce features of parallel electric fields, electron distributions, ion distributions, and wave turbulence seen in satellite observations in the auroral upward-current region and, for the first time, demonstrate that auroral acceleration can be driven by a parallel electric field supported, in part, by a quasistable, strong double layer. In addition, the simulations verify that the streaming interaction between accelerated O^+ and H^+ populations continuously replenished by the double layer provides the free energy for the persistent formation of ion phase-space holes.

PACS numbers: 94.30.cq, 52.35.Fp, 94.05.Lk

The upward-current region of the auroral zone [1] is characterized by earthward traveling electrons associated with visible arcs generated when the electrons collisionally excite atoms in the lower ionosphere. There are at least two boundaries associated with the upward-current region [1]: a low-altitude boundary that separates the ionospheric plasma from the auroral-cavity plasma and a high-altitude boundary that separates the magnetospheric plasma from the auroral-cavity plasma. This Letter focuses on the low-altitude boundary. Among the defining characteristics of the auroral cavity are a factor of ~ 10 density depletion relative to the adjacent ionosphere, and the presence of an antiearthward ion beam. In addition, ion phase-space holes [2] and other localized nonlinear structures [3] have been observed in the auroral cavity.

Parallel electric fields have been established as the primary source for the acceleration of auroral electrons [1,4]. One of the outstanding questions of auroral physics is how these fields are self-consistently supported in a collisionless plasma. Observations from the Polar [5,6] and Viking [7,8] satellites have been made of large-amplitude (a few tens to hundreds of mV/m), localized parallel electric fields (~ 10 electron Debye lengths parallel to the geomagnetic field, $\mathbf{B}_0$). At lower altitudes (~ 4000 km), the Fast Auroral SnapshoT (FAST) [1] satellite has measured large-amplitude (hundreds of mV/m), localized parallel electric fields at the ionosphere-auroral-cavity boundary (IACB). The electric field associated with the IACB was shown [9] to be consistent with a double layer (DL) [10,11] constructed using methods similar to those of Bernstein, Greene, and Kruskal (BGK) [12].

The BGK DL models are *stationary* solutions of the Vlasov-Poisson system, but there is no guarantee that any particular solution is *stable*. Therefore, the primary question that we address in this Letter is whether the parallel electric fields at the IACB can be supported by a DL that is at least *quasistable*. Additionally, we address whether the DL is consistent with the observed features of the boundary

region, including the density depletion across the IACB and the intense turbulence inside the auroral cavity. To perform this study, we initialize 1D and 2D Vlasov simulations with a model BGK DL based closely on observations [9]. This work advances on previous studies [13–15] modeling the interactions of accelerated H^+ and O^+ ions by self-consistently including an observationally based accelerating DL electric field in the simulations.

Figure 1 displays observations of an auroral cavity crossing from FAST and illustrates the basic features of the IACB. Panels a and b show the parallel and perpendicular electric fields at two bandwidths, 16 (red) and 256 Hz (black). The H^+ gyrofrequency is ~ 200 Hz. Stronger fluctuations in the 256 Hz bandwidth trace are adjacent to the IACB. The ion and electron energy fluxes are displayed in panels c and d. The ion beam at ~ 1 keV (panel c) clearly indicates that FAST is inside the auroral cavity. Before and after the ion beam is observed, the satellite is in the ionosphere-dominated plasma. The negative unipolar pulses in $E_\parallel$ (panel a) correspond to crossings of a DL that separates the ionosphere and auroral cavity. The unipolar pulses of opposite polarity in $E_\perp$ (panel b) that are seen when FAST enters and exits the auroral cavity—although less localized in the latter case—indicate that the DLs are *oblique* to $\mathbf{B}_0$, corresponding to the two sides of an inferred large-scale U-shaped electrostatic potential structure [1]. Panel e displays a factor of ~ 10 density depletion inside the auroral cavity.

The goal of the BGK initialization of the simulations is to find candidate distribution functions that self-consistently support the parallel electric field of a DL in order to study the dynamic evolution and stability of the DL. We find solutions of the stationary Vlasov-Poisson system by specifying all of the distribution functions bordering the DL on both the ionosphere and auroral-cavity sides subject to constraints of global charge neutrality, as well as local neutrality asymptotically far from the DL. These distributions, $f(\phi, v_z)$, are functions of electrostatic
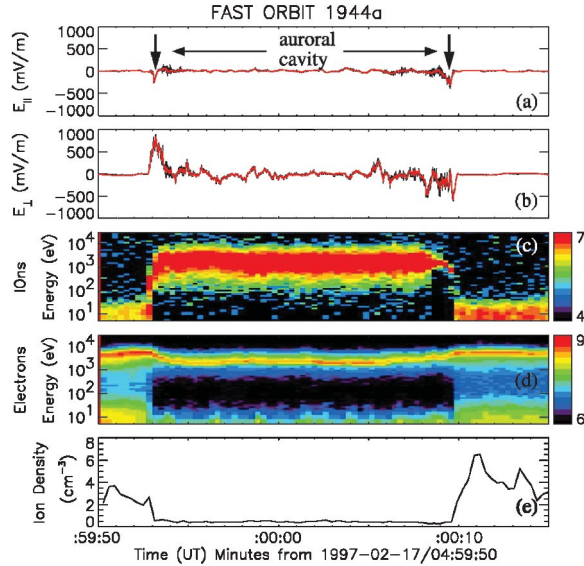
FIG. 1 (color). (a) Parallel and (b) perpendicular electric fields at two different band widths: 256 (black) and 16 Hz (red). (c) Ion and (d) electron energy flux, in units of log(eV/cm² s sr eV) and (e) ion density. The vertical black arrows in panel (a) indicate the IACB crossings.

potential and parallel velocity only [16], and dependence on position (parallel to $\mathbf{B}_0$) is implicit in the assumed single-valued (i.e., monotonic) mapping between ϕ and z. Specifically, we use a pseudopotential method [17] to find $z(\phi)$, and invert to find $\phi(z)$. Once $\phi(z)$ is found we then map the distribution functions $f(\phi[z], v_z) \rightarrow f(z, v_z)$, which are used to seed the Vlasov simulations.

The initial distribution functions are based on FAST data [9] and include flat-topped ionospheric and auroral-cavity electron populations, antiearthward flowing ionospheric H⁺ and O⁺ ions modeled as cold (40 eV) Maxwellians with drifts of twice their respective thermal velocities, and a hot (2500 eV) auroral-cavity H⁺ population modeled as a nondrifting Maxwellian. We also include a cold (45 eV), trapped ionospheric electron population that is excluded from the auroral cavity by the DL potential barrier, as evident in the observations of Fig. 1(d). The total potential drop across the DL is specified to be 1000 V, which is within the range of observed values.

The 1D Vlasov simulation is performed in z-v_z phase space using the time-splitting method of Cheng and Knorr [18]. In the open boundary simulations, the distribution functions near the boundaries are replaced by weighted averages of the evolved and boundary distributions (fixed at their initial values) to prevent the build up of sheaths and sharp gradients. We set, $\phi = E_z = 0$ at the left (iono-spheric) boundary, which is assumed not to be strongly in-fluenced by the evolution of the plasma in the interior of the simulation box. For $z > 0$, the field E_z and the potential ϕ are evaluated as the first two integrals of the charge den-sity. Total charge neutrality in the simulation domain is not imposed, but any electric field at the right (auroral cavity)

boundary that develops from a net charge imbalance tends to act self-consistently so as to restore neutrality.

The phase-space domain is established on a $N_z \times N_{v_z} = 2048 \times 640$ grid that spans the regions $0 \leq z \leq 90$ km and $-180 v_s \leq v_z \leq 180 v_s$, where v_s is the velocity of a 1 eV particle of species s. Because the Debye length changes throughout the simulation box, we have chosen to use physical units, which also aids in comparisons with obser-vations. Based on the ionospheric ion population, the box length is ~2000 Debye lengths. However, based on the hot, auroral-cavity electrons (using the second moment as a proxy for temperature), the box length is ~270 Debye lengths. The mass ratios in the 1D simulation are physical: $M_H/m_e = 1836$ and $M_H/M_O = 16$. The total duration of the simulation run is ~4500 electron ionospheric plasma periods $(2\pi/\omega_e)$, or ~1/2 second for typical densities.

The evolution of the electric field from the 1D simula-tion can be seen in the time history shown in Fig. 2. The initial BGK DL, which is the unipolar (red) stripe near $z = 21.5$ km remains quasistable during most of the simula-tion. The ionosphere (auroral cavity) lies to the left (right) of the DL. The diagonal bipolar fields with $dz/dt > 0$ are the signatures of ion phase-space holes (discussed further in connection with Fig. 3), which propagate away from the DL. Because the dominant instability is undergoing linear growth from noise, very little change is evident until $\omega_e t \approx 5000$. At $\omega_e t \approx 8000$, H⁺ phase-space holes begin to form at and above $z \approx 45$ km. At about the same time, a strong bipolar electrostatic structure forms near $z = 45$ km and travels earthward toward the DL. This bipolar structure has the polarity of an electron hole but, based on its phase-space properties (discussed below), is tentatively identified as an ion-acoustic soliton. This electrostatic structure and the H⁺ holes are interrelated in that as the solitonlike structure propagates toward the DL, so does the point of origin of the holes. At $\omega_e t \approx 2.3 \times 10^4$, the electrostatic structure hits and interacts with the DL. This interaction weakens the DL but does not destroy it.

Further insight into the evolution of the plasma can be gained by examining the phase-space distributions at $\omega_e t = 11\,500$ shown in Fig. 3. The DL lies between the two vertical lines. At this stage in the simulation, H⁺ ion holes are evident as the circular vortexlike structures. The
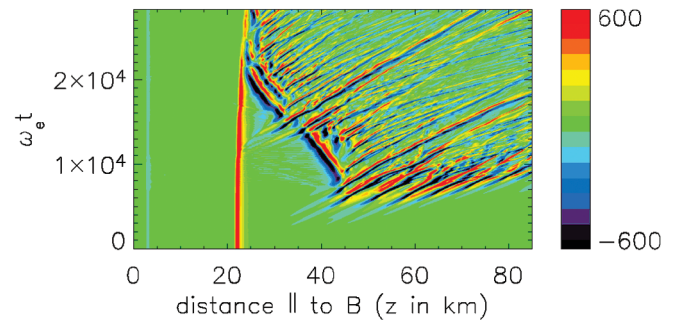
FIG. 2 (color). Time history of the electric field from the 1D simulation. The color scale indicates field amplitude in mV/m.
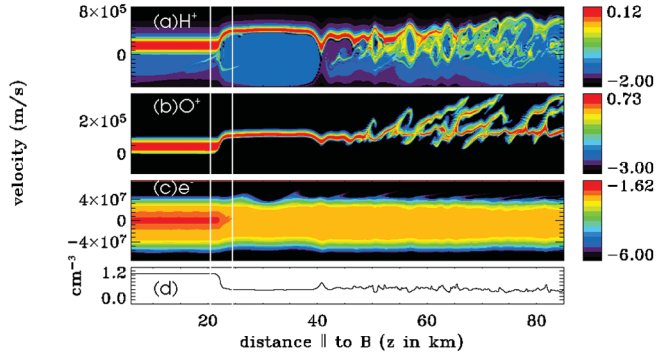
FIG. 3 (color).   Phase-space plots of H^+ (a), O^+ (b), and e^- (c), and ion density plot (d), all at $\omega_e t = 11\,500$.

dominant linear instability in the simulation is driven by the relative drift between the H^+ and O^+ beams accelerated into the auroral cavity by the DL. The DL accelerates both ion species to the same energy, giving the O^+ beam a velocity that is $1/4$ the H^+ beam velocity. For the parameters of this simulation, the instability is reactive (i.e., fluid-like), with the thermal widths of the ion beams small compared to their relative drift [19].

The linear growth saturates when part of the H^+ population becomes trapped in the wave potential which then leads to the nonlinear formation of the ion phase-space holes. The O^+ distribution does not become trapped because the wave potential saturates below the O^+ trapping threshold. Ion holes, such as the large one near $z = 58$ km in Fig. 3(a) are characterized by a low phase-space density on the most deeply trapped orbits relative to the less deeply trapped orbits, resulting in a negative charge density near the center of the hole (in z) and a positive charge density on the "wings" as in Fig. 3(d). Integrating this tripolar charge density leads to the bipolar electric-field structure seen in Fig. 2. Because the DL is quasistable for the duration of the simulation, there is a continual replenishment of the relatively drifting H^+ and O^+ ion beams, allowing ion holes to persist for the duration of the simulation.

The structure that we have tentatively identified as an ion-acoustic soliton is also evident in the ion phase-space plots. Because its bipolar field corresponds to a positive potential "spike", the ion beams slow down and their densities increase as a consequence of flux conservation. This velocity decrease and density increase are seen near $z = 39$ km in frames a, b, and d of Fig. 3. In addition, a bulge in the electron phase-space distribution can be seen at the same location in Fig. 3(c), which shows that this structure is not an electron hole because the trapped electron orbits are all filled. (Electron holes, like ion holes, exhibit a depletion of phase-space density on deeply trapped orbits). The ion density diagnostic also reveals that the density depletion in the auroral cavity is preserved well into the nonlinear stage of the simulation.

To verify that the features observed in the 1D simulations are not artifacts of the limited geometry, we extended the simulation studies to a 2D domain, where the effects of

the geomagnetic field are included. The H^+ and O^+ ions are treated as weakly magnetized and the electrons as infinitely magnetized. The ion phase-space evolution perpendicular to $\mathbf{B}_0$ uses a reduced algorithm in four dimensions (rather than five dimensions) phase space [20]. Therefore, the perpendicular evolution is not fully kinetic. Despite this limitation, the wave vector and growth rate of the fastest-growing mode in a doubly periodic 2D simulation initialized with the auroral-cavity distributions are found to agree well with the predictions of linear kinetic theory.

Because satellite observations indicate that oblique DLs are common in the upward-current region [1], we have chosen to initialize a 2D simulation with a DL aligned with the axes of the simulation box, but with a magnetic field $\mathbf{B}_0$ oblique to the DL normal. An obliqueness angle of $\theta = 45°$ is chosen, consistent with observations. We consequently employ two complementary coordinate systems: z-y relative to the spatial grid of the simulation vs z'-y' relative to $\mathbf{B}_0$. Since all velocity coordinates in phase space are orthogonal to all spatial coordinates, we represent the hydrogen distribution as $f_H(z, y, v_{z'}, v_{y'}, v_{x'})$ and likewise for f_O. The Vlasov equation is evolved numerically by projecting $(E_z, E_y) \rightarrow (E_{z'}, E_{y'}) \equiv (E_\parallel, E_\perp)$ via a rotation through angle θ, updating the velocity distributions, and then projecting $(v_{z'}, v_{y'}) \rightarrow (v_z, v_y)$ via the inverse rotation and updating the spatial distributions.

The simulation is performed on a spatial grid of $N_z \times N_y = 384 \times 64$ points and a velocity grid of 256 points in $v_{z'}$ spanning the same range as in 1D $(-180 v_s \leq v_{z'} \leq 180 v_s)$. The perpendicular velocity distribution for each ion species in the context of our reduced Vlasov model is represented by 32 equally spaced points in azimuth φ on a ring of constant $|v_\perp|$, so that $v_{x'} = v_\perp \cos\varphi$ and $v_{y'} = v_\perp \sin\varphi$. The radius of the ring is proportional to the effective perpendicular thermal velocity, which does not evolve in our reduced simulation scheme. We have chosen perpendicular temperatures $T_{H\perp} = 100$ eV and $T_{O\perp} = 150$ eV based on FAST observations in the auroral cavity. The spatial grid spans the domain $0 \leq z \leq 34$ km and $0 \leq y \leq 12$ km. The mass ratio used in the 2D magnetized simulation is $M_H/m_e = 400$ and $M_O/M_H = 16$, with the magnetic field strength chosen so that $\Omega_H/\omega_H = 1/4$, corresponding to an H^+ gyroradius of ~ 420 m.

The initial 2D DL is specified with the same potential as in the 1D simulation (i.e., $\phi_{2D}[z, y] = \phi_{1D}[z]$). The initial distributions are gyrotropic in φ (for magnetized ions), with $f_{2D}(z, y, v_{z'}, \varphi) \propto f_{1D}(z, v)$. We note, however, that because of the finite ion gyroradii, this is not a true BGK DL solution (except for $\theta = 0$), and the oblique DL does in fact weaken in the 2D simulation, although it does eventually stabilize.

Snapshots of $E_\parallel$ and $E_\perp$ at $\omega_e t \approx 6000$ are shown in Fig. 4(a) and 4(b). At the same time, a reduced phase-space plot (averaged over φ) of H^+ at $y = 0$ is shown in panel c. Phase-space holes have formed as evidenced by the bipolar structures in $E_\parallel$ and by the trapped ions in H^+ phase space.
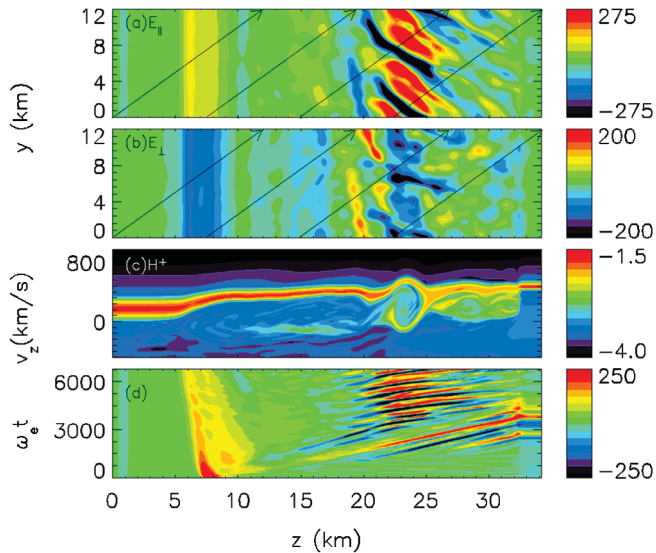
FIG. 4 (color). 2D simulation results showing snapshots at $\omega_e t = 6000$ of (a) $E_\parallel$, (b) $E_\perp$, (c) reduced H^+ phase space at $y = 0$ averaged over φ, and (d) time history of $E_\parallel$ at $y = 0$. Black vectors (a and b) indicate the direction of **B**.

Panel d shows a time history of $E_\parallel$ at $y = 0$ analogous to Fig. 2. The dominant linear electrostatic instability in a 2D magnetized plasma is oblique to the geomagnetic field and is due to the coupling of the fast O^+ cyclotron with the slow H^+ cyclotron mode [21]. Just as in 1D, the 2D instability saturates by trapping of the H^+ ions, which leads to the formation of phase-space holes near $\omega_e t = 1500$. The initial holes have little structure in y, reflecting the corresponding lack of structure in y (except for noise) in the DL itself. However, as the transverse electric-field perturbations grow, the holes break up (starting near $\omega_e t = 3000$) and align primarily along y' while moving parallel to z', as in Fig. 4(a).

A solitonlike feature does not form in this 2D simulation, due to the weakening of the initial non-BGK DL potential [Fig. 4(d)]. A related simulation run with a lower perpendicular ion temperatures resulted in less weakening of the DL and the formation of solitonlike structures similar to those in the 1D simulation. An analysis as to the conditions under which such structures form is the subject of ongoing research.

The results of the 1D and 2D simulations share a number of features with the observations. For example, the evolved DL has a parallel size that is about the same as observed DLs (~ 4 km). Electric-field amplitudes of the ion holes are also about 2–4 times larger in the simulations (~ 400 mV/m) than typically observed (~ 100–200 mV/m) [2]. We note, however, that the amplitude of the typical hole electric field decreases with distance from the DL in the simulations so that the short simulation box size may bias the above estimate toward larger amplitudes. Additional qualitative similarities between the evolved simulations and observations include the presence of ion beams and the lack of cold electrons in the auroral cavity.

In conclusion, the Vlasov simulations presented in this Letter show that the dynamic evolution of BGK DL models of the IACB are quasistable. These simulations further demonstrate the fundamental relationship between DLs and other nonlinear structures such as ion holes.

*Present address: Los Alamos National Laboratory, Los Alamos, New Mexico 87545, USA.

[1] R. E. Ergun, L. Andersson, D. Main, Y. J. Su, C. W. Carlson, J. McFadden, and F. S. Mozer, Phys. Plasmas **9**, 3685 (2002).

[2] J. P. McFadden, C. W. Carlson, R. E. Ergun, F. S. Mozer, I. Roth, and E. Möbius, J. Geophys. Res. **108**, 8018 (2003).

[3] R. Pottelette and R. A. Treumann, Geophys. Res. Lett. **32**, L12 104 (2005).

[4] F. S. Mozer, C. W. Carlson, M. K. Hudson, R. B. Torbert, B. Parady, J. Yatteau, and M. C. Kelley, Phys. Rev. Lett. **38**, 292 (1977).

[5] F. S. Mozer and C. A. Kletzing, Geophys. Res. Lett. **25**, 1629 (1998).

[6] A. J. Hull, J. W. Bonnell, F. S. Mozer, and J. D. Scudder, J. Geophys. Res. **108**, 1007 (2003).

[7] L. P. Block, C. G. Fälthammar, P. A. Lindqvist, G. Marklund, F. S. Mozer, A. Pederson, T. A. Potemra, and L. J. Zanetti, Geophys. Res. Lett. **14**, 435 (1987).

[8] P. A. Lindqvist and G. T. Marklund, J. Geophys. Res. **95**, 5867 (1990).

[9] R. E. Ergun, L. Andersson, D. Main, Y. J. Su, D. L. Newman, M. V. Goldman, C. W. Carlson, J. P. McFadden, and F. S. Mozer, Phys. Plasmas **9**, 3695 (2002).

[10] L. P. Block, Astrophys. Space Sci. **55**, 59 (1978).

[11] M. A. Raadu, Phys. Rep. **178**, 25 (1989).

[12] I. B. Bernstein, J. M. Greene, and M. D. Kruskal, Phys. Rev. **108**, 546 (1957).

[13] J. P. Crumley, C. A. Cattell, R. L. Lysak, and J. P. Dombeck, J. Geophys. Res. **106**, 6007 (2001).

[14] P. C. Gray, M. K. Hudson, R. Bergmann, and I. Roth, Geophys. Res. Lett. **17**, 1609 (1990).

[15] I. Roth, M. K. Hudson, and R. Bergmann, J. Geophys. Res. **94**, 348 (1989).

[16] H. Schamel and S. Bajarbarua, Phys. Fluids **26**, 190 (1983).

[17] D. R. Nicholson, *Introduction to Plasma Theory* (John Wiley & Sons, New York, 1983), p. 174.

[18] C. Z. Cheng and G. Knorr, J. Comput. Phys. **22**, 330 (1976).

[19] R. Bergmann and W. Lotko, J. Geophys. Res. **91**, 7033 (1986).

[20] D. L. Newman, M. V. Goldman, R. E. Ergun, L. Andersson, and S. N., Comput. Phys. Commun. **164**, 122 (2004).

[21] R. Bergmann, I. Roth, and M. K. Hudson, J. Geophys. Res. **93**, 4005 (1988).